Manuscript prepared for Atmos. Chem. Phys.
with version 5.0 of the LaTeX class copernicus.cls.
Date: 26 March 2014

A Tropical West Pacific OH minimum and implications for stratospheric composition

M. Rex[1], I. Wohltmann[1], T. Ridder[2], R. Lehmann[1], K. Rosenlof[3], P. Wennberg[4], D. Weisenstein[5], J. Notholt[2], K. Krüger[6,*], V. Mohr[6], and S. Tegtmeier[6]

[1]Alfred Wegener Institute for Polar and Marine Research, Potsdam, Germany
[2]Institute of Environmental Physics, University of Bremen, Bremen, Germany
[3]NOAA ESRL Chemical Sciences Division, Boulder, CO, USA
[4]California Institute of Technology, Pasadena, CA, USA
[5]Atmospheric and Environmental Research, Inc., Lexington, MA, USA
[6]Helmholtz Centre for Ocean Research Kiel (GEOMAR), Kiel, Germany
[*]now at: University of Oslo, Oslo, Norway

Correspondence to: M. Rex (markus.rex@awi.de)

Abstract. Most of the short-lived biogenic and anthropogenic chemical species that are emitted into the atmosphere break down efficiently by reaction with OH and do not reach the stratosphere. Here we show the existence of a pronounced minimum in the tropospheric column of ozone over the West Pacific, the main source region for stratospheric air, and suggest a corresponding minimum of the tropospheric column of OH. This has the potential to amplify the impact of surface emissions on the stratospheric composition compared to the impact when assuming globally uniform OH conditions. Specifically, the role of emissions of biogenic halogenated species for the stratospheric halogen budget and the role of increasing emissions of SO_2 in South East Asia or from minor volcanic eruptions for the increasing stratospheric aerosol loading need to be reassessed in light of these findings. This is also important since climate change will further modify OH abundances and emissions of halogenated species. Our study is based on ozone sonde measurements carried out during the TransBrom cruise with the RV Sonne roughly along 140–150° E in October 2009 and corroborating ozone and OH measurements from satellites, aircraft campaigns and FTIR instruments. Model calculations with the GEOS-Chem Chemistry and Transport Model (CTM) and the ATLAS CTM are used to simulate the tropospheric OH distribution over the West Pacific and the transport pathways to the stratosphere. The potential effect of the OH minimum on species transported into the stratosphere is shown via modeling the transport and chemistry of CH_2Br_2 and SO_2.

1 Introduction

The overall composition of the stratosphere is mainly determined by species that ascend from the surface through the troposphere into the stratosphere. Reactions with OH radicals in the troposphere break down many short-lived species into soluble products, that are removed by rainout or deposition on ice that forms near the temperature minimum at the tropopause (WMO, 2011). Hence, the presence of OH in the troposphere shields the stratosphere from many surface emissions and is particularly relevant for compounds that do not photolyse efficiently.

Some important studies were based on fixed uniform mixing ratios of OH or fixed lifetimes of the species that are destroyed by OH in the past (Liang et al., 2010; WMO, 2011, cf. chapter 1.3.3). But the degree of temporal and spatial variability of tropospheric OH is subject of ongoing debate (Hanisco et al., 2001; Lelieveld et al., 2004; Berglen et al., 2004; Manning et al., 2005; Rohrer and Berresheim, 2006; Montzka et al., 2011). There are still systematic discrepancies between models and observations for the spatial distribution of OH (Naik et al., 2013). The variability of OH is key not only for the supply of chemical species to the stratosphere but also for the atmospheric lifetimes of many greenhouse gases and for deriving their source terms from measurements of their atmospheric abundances (Manning et al., 2005).

A major source of OH in clean tropospheric air is formation through:

$$O_3 + h\nu \rightarrow O(^1D) + O_2 \quad \text{(R1)}$$

$$O(^1D) + H_2O \rightarrow OH + OH \quad \text{(R2)}$$

This couples the OH concentration and hence the oxidizing capacity of tropospheric air closely to the ozone concentration (Levy II, 1971; Jaeglé et al., 2001). The OH concentration further depends on the concentration of NO, which controls the conversion of HO_2 into OH:

$$HO_2 + NO \rightarrow OH + NO_2 \quad \text{(R3)}$$

Reactions (R1) and (R2) provide an efficient loss mechanism for ozone (Liu et al., 1983). The efficiency is a function of actinic fluxes at $\lambda < 340\,\mathrm{nm}$ (in clear sky conditions mostly determined by overhead ozone and solar zenith angle) and concentration of water vapor, with higher air temperatures corresponding to higher water concentrations and faster ozone loss.

This favors ozone loss over the westernmost tropical Pacific, where marine boundary layer air temperature is highest globally and overhead ozone lowest (e.g. Kley et al., 1996). Odd oxygen (O_3+O) lifetime (which determines the effective lifetime of ozone) drops to less than a week under these conditions near the surface (e.g. Kley et al., 1996). The odd oxygen lifetime increases steeply with altitude due to decreasing temperature which leads to lower water vapor.

High sea surface temperatures also favor strong convective activity in the tropical West Pacific, which can lead to low ozone mixing ratios in the convective outflow regions in the upper troposphere in spite of the increased lifetime of odd oxygen.

Due to the general low and mid-tropospheric advection from the east by the Walker circulation across the vast Pacific, air above the tropical westernmost Pacific has been in a clean, warm and humid environment for a long time and loss of odd oxygen and of ozone precursors like NO_x ($= NO + NO_2$, NO_x is lost by conversion into HNO_3 followed by washout) proceeded longer than elsewhere in the tropics.

The Western Pacific warm pool is also the major source region for stratospheric air (e.g. Newell and Gould-Stewart, 1981; Fueglistaler et al., 2004). Hence, the region of short odd oxygen lifetimes and the source region of stratospheric air are coincident.

Removal of species depends on the oxidation efficiency along the air mass trajectories between the boundary layer and the tropopause. Near the tropical tropopause, air masses go through their temperature minimum, denoted the Lagrangian Cold Point (LCP), experience their final condensation of water and the last removal of soluble species by deposition takes place (e.g. Fueglistaler et al., 2004). Any later breakdown of species can only change the stratospheric balance between species but not the total budgets of e.g. halogens or sulfur. It has been shown that most air masses reach their LCP above the West Pacific (Fueglistaler et al., 2004; Bonazzola and Haynes, 2004; Krüger et al., 2008) and we will show here that the source region in the boundary layer and the transit region in the troposphere are also situated in the same region.

In Section 2 we present ozone sonde measurements carried out during the TransBrom cruise with the RV Sonne roughly along 140–150° E in October 2009. Corroborating ozone measurements are from the TES and OMI/MLS satellite instruments, from other ozone sondes launched in the tropics and from FTIR and lidar instruments. In addition, OH measurements from the STRAT and PEM-Tropics B aircraft campaigns are discussed. These data show a pronounced ozone minimum in the West Pacific and suggest a OH minimum in the same region. In Section 3 we show that the GEOS-Chem CTM simulates a corresponding OH minimum in the West Pacific and that GEOS-Chem compares well to existing measurements. In Section 4 we show trajectory calculations that confirm that the main source region for stratospheric air is coincident with the OH minimum. In Section 5 we show the effect of the low OH values on species that are transported into the stratosphere at the example of CH_2Br_2 and SO_2. The conclusions are given in Section 6.

2 Measurements of OH and ozone

2.1 Ozone profile measurements

Information on tropospheric ozone profiles from the Western Pacific warm pool has been limited so far. Measurements from the south east edge of the warm pool in 1993 carried out on the Research Vessel (RV) Vickers and on Christmas Island during the CEPEX campaign (Kley et al., 1996; Lawrence et al., 1999) and lidar measurements carried out during the PEM-Tropics B campaign onboard the NASA DC-8 aircraft (Browell et al., 2001, Plate 5) show extremely low ozone in the marine boundary layer and in the upper troposphere, the main outflow region of convection. Individual profiles from the stations Samoa, Fiji, Tahiti and Christmas Island further south east (Solomon et al., 2005; Takashima et al., 2008) and from Indonesian stations Pontianak and Kototabang slightly to the west (Fujiwara et al., 2003) also show very low ozone values, typically occuring in some ten percent of the measurements. Kley et al. (1996) derived a reduced oxidizing capacity of the tropopause region above the Central Pacific from his data.

Figure 1 shows our tropospheric ozone mixing ratios determined by sonde measurements conducted during the TransBrom cruise with the RV Sonne roughly along 140–150° E in October 2009 (Krüger and Quack, 2013). In all six profiles in the central part of the warm pool between 15° N and 10° S ozone was at or below the detection limit throughout the troposphere (about 15 ppb, see Appendix A for discussion of the detection limit and robustness of the mea-

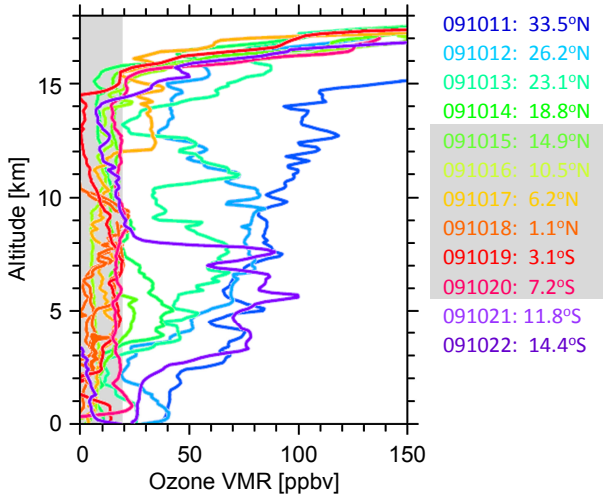

Fig. 1. West Pacific tropospheric ozone mixing ratios from balloon sondes as a function of altitude. The legend shows date and latitude of each sounding. Gray shading indicates detection limit (left) and soundings with ozone abundances mostly below the detection limit (right).

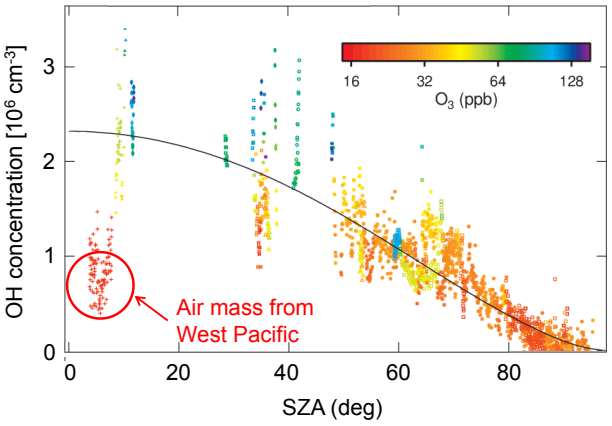

Fig. 2. OH vs. solar zenith angle (SZA) for measurements above 11 km during STRAT (10 s averages). Color indicates ozone mixing ratio. The black line represents the compact relation reported by Hanisco et al. (2001). The red circle indicates air masses from the West Pacific with extremely low ozone and OH. For these air masses NO is also extremely low (below 10^8 molecules cm^{-3}, not shown).

surements). The measurements are confirmed by simultaneous FTIR measurements of ozone on the RV Sonne (Ridder et al., 2012). Figure 5 in Ridder et al. (2012) shows excellent agreement between ozone columns from ozone sondes and the FTIR instrument.

Loss in the boundary layer combined with convectively driven vertical mixing is the most likely explanation for the near zero values of ozone throughout the troposphere (see also Browell et al., 2001; Kley et al., 1996; Solomon et al., 2005).

Note that the CEPEX data has been analyzed based on a correction due to the electrical background current in the ozone sonde measurement cell that is now believed to lead to an underestimate of the real ozone abundance and has a considerable low bias compared to our measurements (Vömel and Diaz, 2010). The result of running our raw data through an analysis similar to the one used for the CEPEX data defines the lower limit of the uncertainty range shown in Fig. A1 in Appendix A. This approach used with our data results in negative ozone values throughout much of the troposphere for most of our tropical soundings.

Our ozone sonde measurements from the RV Sonne are from the key region of troposphere-to-stratosphere transport (see discussion in Sect. 4) and from the region where satellite measurements show a pronounced ozone minimum (see Sect. 2.3). The PEM-Tropics B measurements and the measurements from the RV Vickers are from the edge of the ozone minimum and the edge of the region of troposphere-to-stratosphere transport.

2.2 Aircraft measurements of OH

In situ measurements of OH during the PEM-Tropics B campaign carried out with the ATHOS instrument on the NASA DC-8 aircraft in a vast region between 150°E and 90°W show typical mixing ratios of OH between 0.1 and 0.2 ppt, with little sign of a spatial gradient (Tan et al., 2001). Unfortunately, the flights just missed the region where our model runs simulate the lowest OH values, but the results agree well with the model results in that region (see Section 3). Note that there is some seasonal variation in OH abundances (e.g. Berglen et al., 2004).

In situ measurements in the tropopause region close to Hawaii during STRAT (Stratospheric Tracers of Atmospheric Transport), a NASA campaign with the ER-2 high altitude research aircraft, include O_3, NO and OH (Fig. 2). A patch of air originating from the convective outflow area in the West Pacific was probed, which was transported to Hawaii by tropopause level advection (red circle in Fig. 2, corresponding air mass trajectory shown in Fig. 3). This air was characterized by extremely low ozone and NO. Low NO further reduces OH concentrations due to Reaction (R3). OH concentrations in this air mass are up to a factor of four smaller than those observed in the compact OH vs. solar zenith angle relation reported by Hanisco et al. (2001) for similar altitudes.

The data was collected using a suite of in situ instruments onboard the NASA ER-2 high-altitude research aircraft during the STRAT field mission, which occurred in the 1995–1996 period. OH and HO_2 were measured with a laser-induced fluorescence instrument (Wennberg et al., 1994). O_3 was measured by a dual-beam UV photometer (Proffitt and

McLaughlin, 1983). Measurements of NO were made with a chemiluminescence detector (Gao et al., 1997). Temperature and pressure were obtained using the onboard meteorological measurement system (Scott et al., 1990). The campaign carried out measurements in the vicinity of Hawaii. During a portion of a flight track at 20.37–22.19° N, 159° W a patch of air was sampled that originated from the ozone minimum in the West Pacific. A 12 day back trajectory of that airmass is shown in Fig. 3. The trajectory was calculated by the ATLAS trajectory model driven by ERA-Interim data (see Sect. 4 for details).

2.3 Satellite measurements of ozone

The ship and aircraft measurements only provide local snapshots of atmospheric conditions. We have used measurements of the satellite borne Tropospheric Emission Spectrometer (TES) to assess the geographical extent and persistence of the tropospheric ozone minimum.

Figure 4a shows the monthly mean tropospheric ozone column for October 2009 from TES. The data are in good agreement with the sonde data (shown as open circles) and combined OMI/MLS satellite data (Ziemke et al., 2006; Joiner et al., 2009), confirming the pronounced tropospheric ozone minimum above the warm pool.

The satellite data show that this feature is persistent and present during all years of TES measurements. Figure 5 shows monthly averaged data for January, April, July, and October for the years 2005–2009. The data show that interannual variability is fairly low. The location of the minimum moves towards the central Pacific during El Niño conditions, which are part of the ENSO variability (El Niño/Southern Oscillation). Both the second half of 2006 and 2009 (October panels) were El Niño periods. The ozone minimum is present year round but shows some annual cycle and is least pronounced in January.

Tropospheric ozone columns for Figs. 4a and 5 were calculated from all available Level 2 profile data by integrating the mixing ratios between the surface and 150 hPa (applying recommended quality checking, see Data User's Guide, Osterman, 2013). Monthly means were calculated by binning the satellite measurements of a particular month. This was done to enable construction of global maps as daily satellite sampling is too coarse with respect to longitude. Differences between satellite and sonde measurements shown in Fig. 4a are within the range of the day to day variations shown by TES.

3 Model calculations of OH and ozone

To further understand the measurements, we used the tropospheric GEOS-Chem Chemistry and Transport Model (CTM) to examine the geographical extent of the tropospheric ozone minimum and of the inferred OH minimum. Model runs were designed to cover the RV Sonne cruise. Details of the model runs are given in Ridder et al. (2012). The spatial extent of the OH minimum is not directly observable by measurements due to a lack of OH measurements.

Figure 4b and c show the modeled distribution of the tropospheric ozone and OH columns in the tropics averaged over the first half of October 2009. Pronounced minima in the tropospheric columns of ozone and OH are present over the westernmost tropical Pacific. Uncertainties of global model calculations are inherently difficult to quantify. The model results shown here are sensitive on clouds and water vapor concentration in the study region. A proper quantification of the uncertainties of the model results would require to propagate the uncertainties of dozens of input parameters and boundary conditions through the model (e.g. Kawa et al., 2009), an approach that is not possible for a global model study. However, Ridder et al. (2012) showed that the GEOS-Chem calculation used here reproduces ozone and CO observations very well. In particular, their Fig. 5 shows excellent agreement between ozone sondes, FTIR measurements and modeled ozone both in the profile and the column. Also, the main features of the ozone distribution are robust among a wide range of tropospheric CTMs (Stevenson et al., 2006). These results increase our confidence in the the ability of GEOS-Chem to reproduce the main chemical mechanisms in the study region well. However, due to the uncertainties mentioned above, to robustly quantify the level of OH in the area of the tropical West Pacific will require comprehensive in-situ measurements of OH in that area.

Figure 6 shows modeled equatorial OH profiles averaged over the first half of October 2009. The area between the green lines shows the region of the OH minimum in Fig. 4c. In the region of the OH minimum, the OH mixing ratio is consistently below 0.1 ppt at all altitudes, and locally even below 0.05 ppt. In the Pacific outside of the OH minimum, where OH measurements were taken onboard the NASA DC-8 during PEM-Tropics B (Tan et al., 2001), typical mixing ratios of 0.1–0.2 ppt are modeled. This compares very well with the OH measurements of Tan et al. (2001) when considering the uncertainty of the measurements and the different time period.

Figure 4 of Berglen et al. (2004) and Figure 1 of Lelieveld et al. (2004) also show low OH values in the boundary layer in the West Pacific for the TM3 and OsloCTM2 tropospheric CTMs, respectively. However, these boundary layer values are not directly comparable to the OH columns shown in Fig. 4c. All of these models show discrepancies in the extent and location of the low OH values. The temporal and spatial variability of tropospheric OH is still subject of an ongoing debate (e.g. Naik et al., 2013). While there is evidence from the good agreement of our model runs with measurements that the OH minimum actually exists, observations of OH in the tropical West Pacific are required to establish a robust basis for assessments of the OH field in this key geographical region.

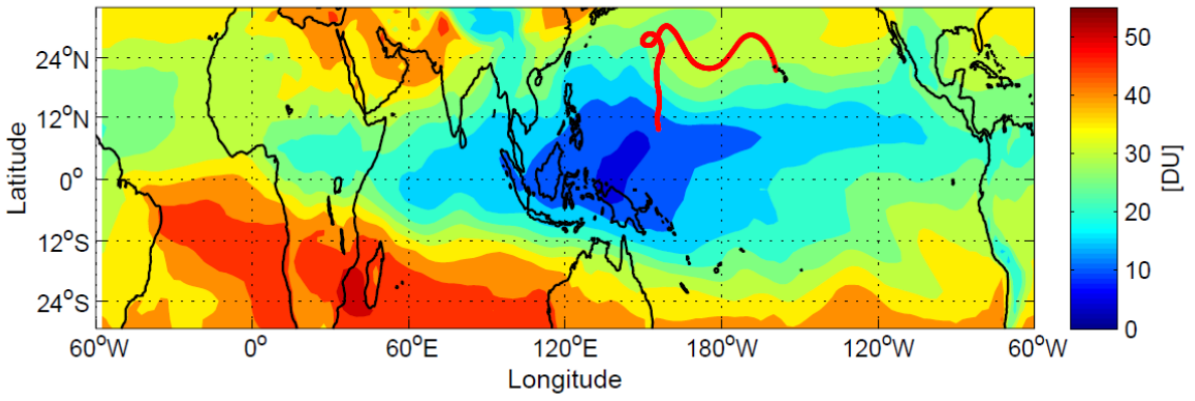

Fig. 3. 12 day back trajectory (red line) ending close to Hawaii of the air mass, which is indicated by the red circle in Fig. 2. Color indicates the tropospheric ozone column from GEOS-Chem as in Fig. 4b.

Sources of uncertainty of our model runs include not only source gas emissions and water vapor abundance, but also details regarding the ozone photolysis (Naik et al., 2013). Photolysis rates will not only be influenced by assumptions on the stratospheric overhead ozone column, but also by the assumptions on clouds, which play a large role in the convectively active West Pacific.

Another modeling study directly related to our results has been performed by Lawrence et al. (1999). Lawrence et al. (1999) were able to reproduce the main features of the ozone profiles measured during CEPEX in the ozone minimum (Kley et al., 1996) with the MATCH-MPIC CTM and conclude that convective pumping is responsible for the low ozone values in the upper troposphere.

4 Air mass origin

We used the Lagrangian Chemistry and Transport Model ATLAS to determine the area in which air masses pass through the troposphere between their last contact with the boundary layer and the LCP (Fig. 4d and Fig. 7) and to calculate the area in the boundary layer where the air masses originate (Fig. 4e and Fig. 8).

ATLAS is a global Chemistry and Transport Model based on a Lagrangian (trajectory-based) transport and mixing scheme (Wohltmann and Rex, 2009; Wohltmann et al., 2010). Here we use the trajectory module of the model in a stand-alone mode. Trajectory calculations are driven by ECMWF ERA-Interim reanalysis data (Dee et al., 2011). The vertical coordinate of ATLAS is a hybrid pressure-potential temperature coordinate. Corresponding vertical motions are calculated from the vertical winds and the heating rates (including clouds) provided by ERA-Interim. For ten years (2002–2011) trajectory runs were started on 400 K on 31 January between 30° S and 30° N on a $2° \times 2°$ grid and run backward in time for 120 days. Time and location of the passages through the LCP and the 800 hPa level (roughly corresponding to the top of the planetary boundary layer) were recorded for every trajectory.

Figure 4d and Fig. 7 show the density distribution function (trajectory air parcels per area) of all locations of the trajectory air parcels between their passage through 800 hPa and their individual LCPs, i.e. all positions in longitude and latitude at every 10 min time step between these passages, regardless of altitude. Figure 4d shows an average over all years, Fig. 7 shows the results for the individual years. Figure 4e and Fig. 8 show the density distribution function for the passages through 800 hPa in the same manner. All values are normalized such that a horizontally uniform distribution corresponds to a value of 1 at every grid point.

The "tropospheric transit region" shown in Fig. 4d correlates with the tropospheric ozone and OH minimum areas discussed above (Fig. 4a–c). This correlation results in a disproportionately large global impact of the OH minimum, in spite of the relatively small size of the minimum. Combining the transport calculations from ATLAS with the chemical fields from GEOS-Chem shows that the average OH concentration for all air masses that ascend into the stratosphere globally (during transport from the boundary layer to the LCP) is only 57 % of the average OH in the 80° W to 100° E and 10° S to 10° N area (outside of the OH minimum). The average OH concentration for the troposphere-to-stratosphere transport was determined by interpolating the GEOS-Chem OH fields on all trajectory positions at every 10 min time step used for Fig. 4d and averaging over all positions.

Some interannual variability can be seen in Fig. 7 and Fig. 8, but there is no clear relation to the ENSO index. The crucial features, like a maximum in the density distribution in Fig. 7 between 120° E to 180° E, are robust. In this paper, we only performed GEOS-Chem model runs for 2009. The interannual variability of the stratospheric input of short-lived species will be examined in a future study.

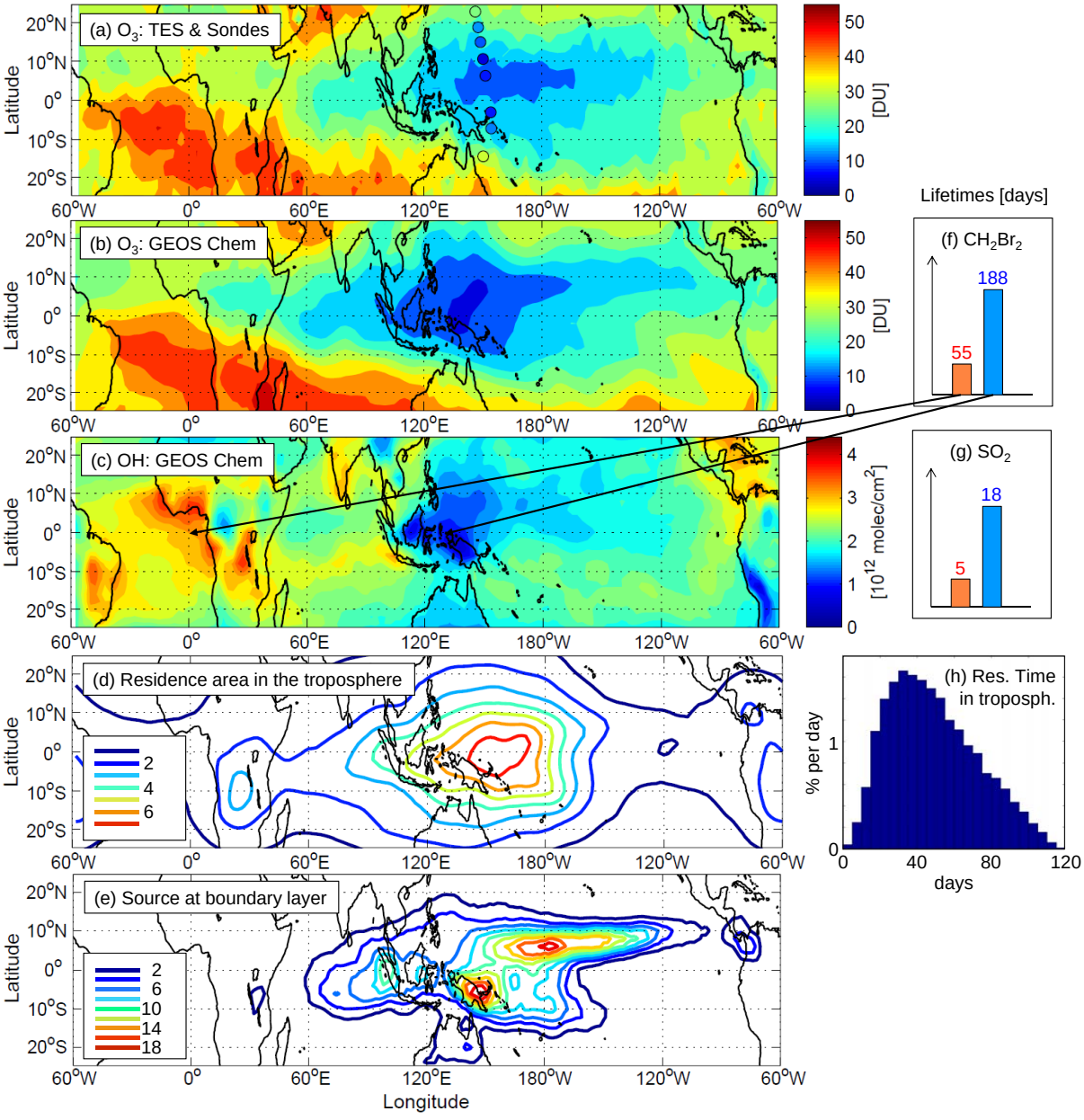

Fig. 4. Tropospheric ozone columns from **(a)** TES for October 2009 (results for 2005–2009 are similar, see Fig. 5), the sondes (open circles, dates see Fig. 1), and **(b)** GEOS Chem (mean 1–15 October 2009). **(c)** OH columns from GEOS-Chem (mean 1–15 October 2009). **(d, e, h)** show ATLAS 4-months backtrajectory runs for air entering the stratosphere (1 October–31 January). Average conditions for 2002–2011, individual results for 2009 in Fig. 7 and Fig. 8. **(d)** Density distribution function of the horizontal positions of the trajectories between the boundary layer and the LCPs. **(e)** Density distribution function of the horizontal positions of the last contact with the boundary layer. The values in **(d)** and **(e)** are normalized such that a horizontally uniform distribution corresponds to a value of 1 at every grid point. **(f–g)** Examples of gas-phase lifetimes of relevant species in the mid-troposphere (500 hPa) at the equator for typical conditions over the Atlantic (0° E, orange) and for conditions in the OH minimum (130° E, blue). **(h)** Distribution of residence times between last contact with the boundary layer and the LCP for trajectories ascending into the stratosphere.

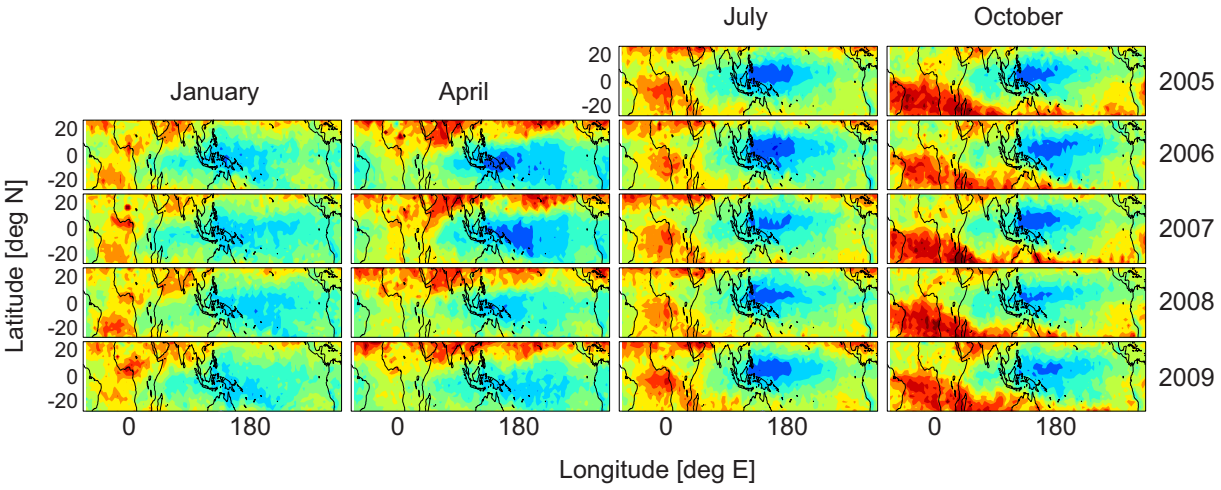

Fig. 5. Monthly mean tropospheric ozone columns from TES for January, April, July and October for the years 2005–2009 as a function of longitude and latitude. Color scale in DU see Fig. 4a.

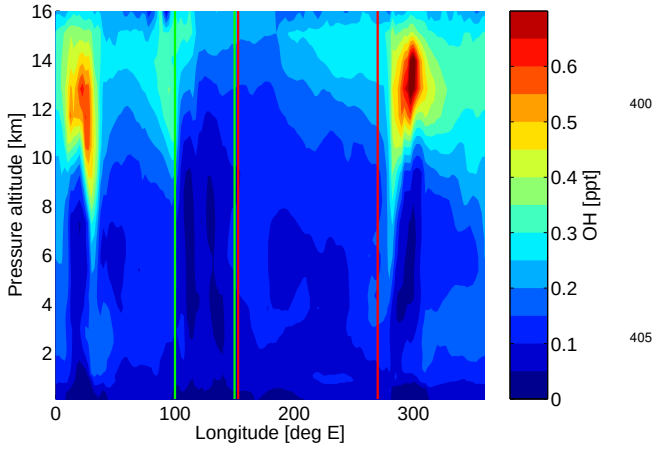

Fig. 6. Cross section of equatorial OH mixing ratio profiles (24 h means) modeled with GEOS-Chem, averaged over the first half of October 2009. The area between the green lines denotes the region of the OH minimum in Fig. 4c. The area between the red lines shows the longitudinal extent of the NASA DC-8 flights of the PEM-Tropics B campaign (which were not always directly at the equator).

5 Lifetimes of chemical species

Figure 4h shows the distribution of the transit times between 800 hPa and the LCP for the trajectories from Fig. 4d in units of the percentage of the trajectories per bin width. Its distribution overlaps the chemical lifetimes of relevant species such as dibromomethane (CH_2Br_2) and sulfur dioxide (SO_2). Hence the fraction of these species that reach the LCP is sensitive to the OH concentrations along their trajectory paths. For further discussion we define an "OH minimum area" (125° E to 140° E) and an "outside minimum area" (80° W to 100° E) in the inner tropics (10° S to 10° N). In the "OH minimum area" the minimum ozone column is only 28 % and the minimum OH column is only 22 % of the respective average column in the "outside minimum area". This has a large impact on lifetimes of chemical species in that region.

5.1 Halogenated species

Short-lived halogenated species are believed to contribute to the stratospheric halogen budget and to amplify polar ozone loss (WMO, 2011). In particular, bromine species are mainly produced by natural biological activity in the oceans (Quack and Wallace, 2003; WMO, 2011). Sources include macroalgae (kelp, seaweed) and phytoplankton (Quack and Wallace, 2003). Increasing seaweed farming in South East Asia, which has been proposed for carbon dioxide sequestration, could contribute to increasing emissions in the future (Martinez-Aviles et al., 2010). In addition, climate change will probably lead to changes in tropospheric OH abundance and halogen emissions (Hossaini et al., 2012).

Short-lived bromine species are thought to contribute roughly 5 ppt (about 25 %) to the stratospheric bromine loading, but with large uncertainties ranging from 1 ppt to 10 ppt in different studies (e.g. Warwick et al., 2006; Liang et al., 2010; Hossaini et al., 2013; Aschmann and Sinnhuber, 2013). Bromine is responsible for a significant part of the heterogeneous ozone depletion in polar spring (WMO, 2011). The most important of the short-lived species are $CHBr_3$ and CH_2Br_2. While $CHBr_3$ is mainly destroyed by photolysis, CH_2Br_2 is mainly destroyed by reaction with OH (e.g. WMO, 2011).

The amount of CH_2Br_2 left at the LCP is a lower limit for the amount of bromine from CH_2Br_2 reaching the stratosphere: While many of the product species of the degradation are soluble and are subject to washout, unsoluble prod-

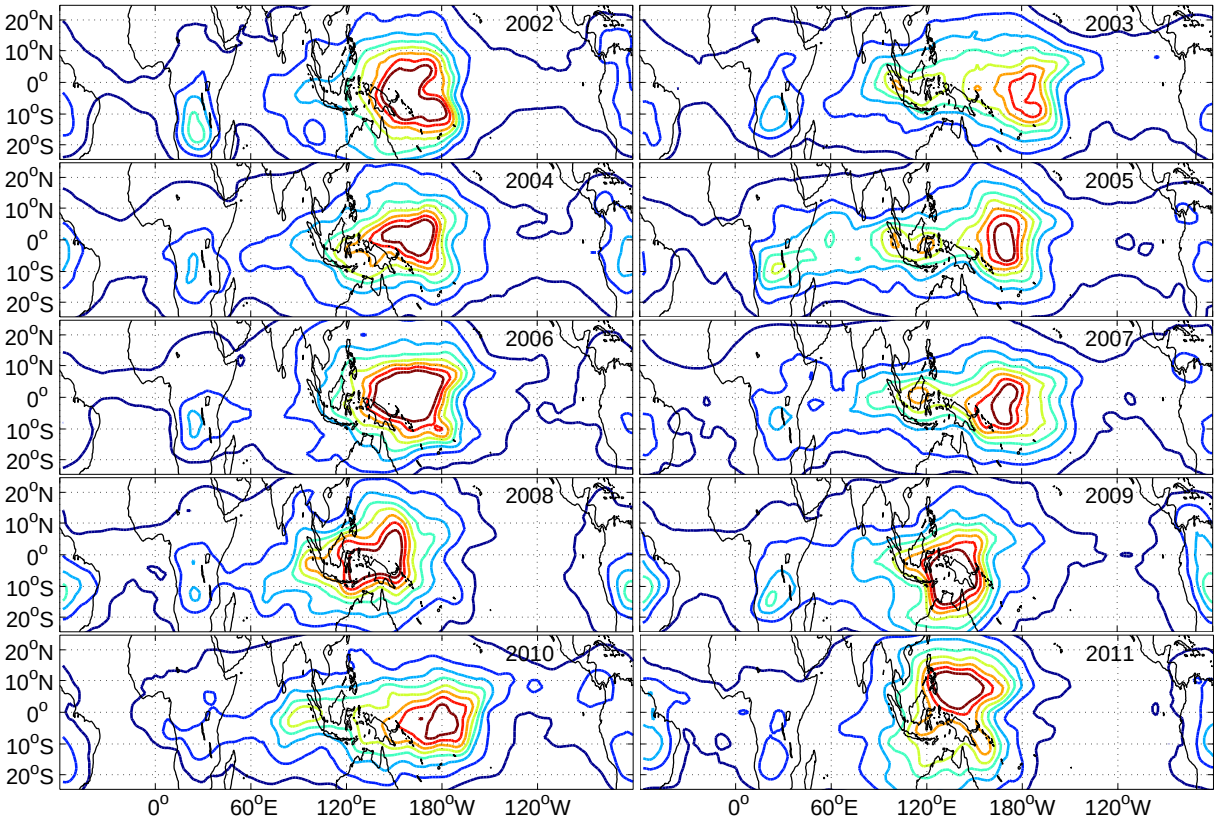

Fig. 7. Density distribution function of the horizontal positions of the trajectories between the boundary layer and the LCPs for all years from 2002–2011. The values are normalized such that a horizontally uniform distribution corresponds to a value of 1 at every grid point. Contours as in Fig. 4d.

uct species and soluble species not washed out can contribute to the stratospheric bromine budget. There are still large uncertainties in the chemistry, washout and adsorption of the product gases of brominated species (e.g. Liang et al., 2010; WMO, 2011; Aschmann and Sinnhuber, 2013).

In addition, emissions are uncertain and emission sources are highly variable in time and space (e.g. Quack and Wallace, 2003; Warwick et al., 2006; Liang et al., 2010; WMO, 2011; Hossaini et al., 2013). However, tropical and coastal regions are thought to play an important role (e.g. Quack and Wallace, 2003; Warwick et al., 2006; Liang et al., 2010). Numerous modeling and measurement studies have tried to better constrain emissions and input into the stratosphere (e.g. Warwick et al., 2006; Liang et al., 2010; Hossaini et al., 2013; Aschmann and Sinnhuber, 2013).

Hence, we will show conceptual results for the lifetime and the loss relative to the initial mixing ratio at 800 hPa here, which are robust quantities.

Figure 4f shows the large difference in CH_2Br_2 lifetime at 500 hPa inside and outside of the "OH minimum area". For the calculation of the lifetimes the reaction with OH and the photolysis were taken into account. Reaction rate constants from Sander et al. (2011) and daily-mean photolysis rates calculated by TUV (Tropospheric Ultraviolet–Visible Model, Madronich and Flocke, 1999) were used. The calculated lifetimes correspond to conditions at 500 hPa above the Equator on 1 October. OH concentrations (24 h means) were assumed to be 7×10^5 molecules cm^{-3} (0.05 ppt) and 24×10^5 molecules cm^{-3} (0.18 ppt), respectively. These values represent the minimum and maximum values determined by the GEOS-Chem model at 500 hPa above the Equator (near 135° E and 0° E, respectively). Under these conditions, the lifetime of CH_2Br_2 is determined almost completely by the reaction with OH, because the photolysis contributes less than 1 % to the CH_2Br_2 loss.

Figure 9 shows that for "outside minimum area" conditions only 30 % of the air masses preserve more than 80 % of the dibromomethane present in the boundary layer, compared to 68 % for "OH minimum area" conditions. Calculations were performed with the same photochemical model as above. The box model was run along each trajectory reaching the stratosphere from the set of trajectories used in Sect. 4. The model was run between 800 hPa and the Lagrangian cold point and results were averaged over all trajectories. The percentage of the CH_2Br_2 reaching the stratosphere was determined by dividing the CH_2Br_2 mixing ratios at

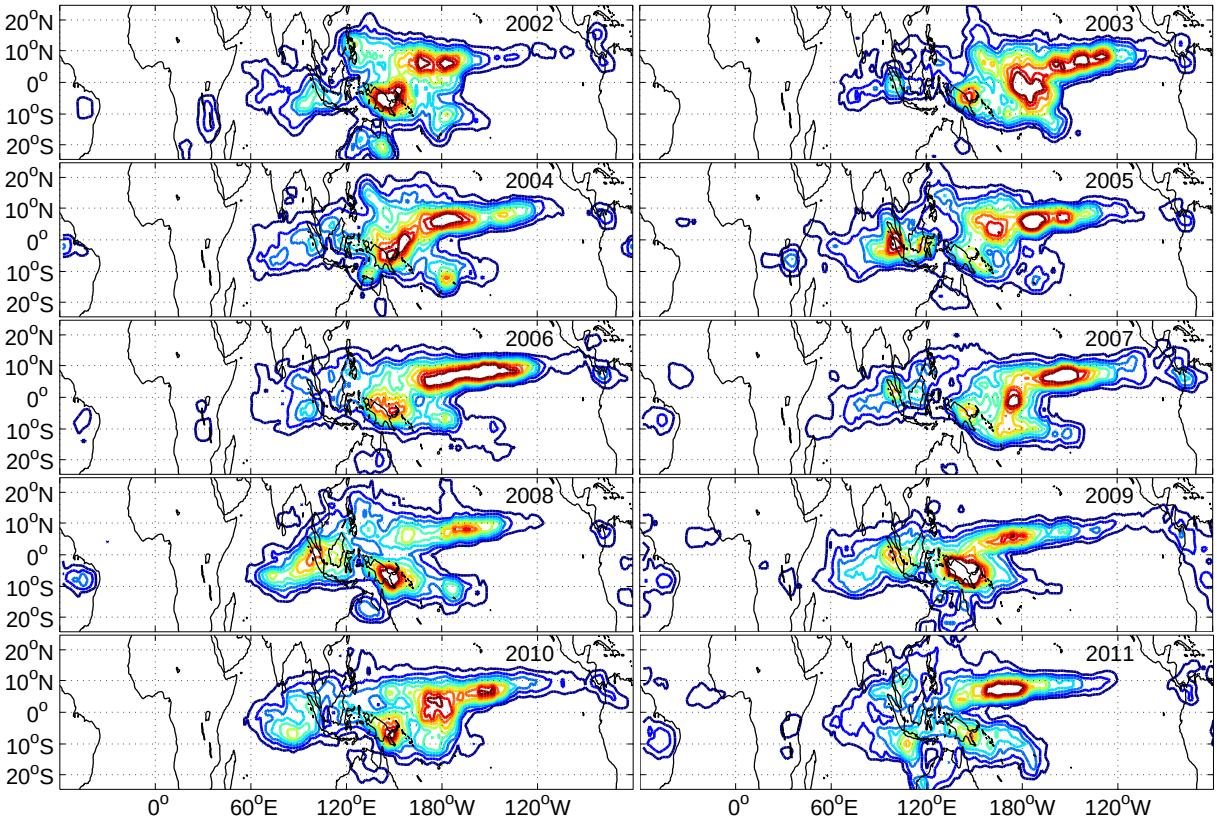

Fig. 8. Density distribution function of the horizontal positions of the last contact with the boundary layer for all years from 2002–2011. The values are normalized such that a horizontally uniform distribution corresponds to a value of 1 at every grid point. Contours as in Fig. 4e.

the LCP by those at 800 hPa. Temperatures along the trajectories were taken from the ERA-Interim reanalysis. OH was determined from the October GEOS-Chem field by averaging model results longitudinally over 125° E–140° E for the "OH hole" conditions and 80° W–100° E for the "outside hole" conditions to give 2-dimensional latitude-pressure fields. These values were interpolated on the trajectories.

5.2 Sulfur dioxide

Furthermore, model calculations suggest a larger impact of increasing anthropogenic emissions of SO_2 in South East Asia (Thomason and Peter, 2006) or of weak to moderate volcanic eruptions (Hofmann et al., 2009; Vernier et al., 2011) on the stratospheric sulfur and aerosol budget in case of low OH values. Stratospheric aerosol is a key element for stratospheric chemistry and has been suggested as a possible contributor to the recently observed decrease in global warming rates (Solomon et al., 2011).

Figure 4g shows gas phase SO_2 lifetimes inside and outside of the "OH minimum area" in the same manner as Fig. 4f for CH_2Br_2, now only considering the reaction of SO_2 with OH.

Figure 10 shows the impact of the OH minimum on the aerosol distribution derived from the AER aerosol model

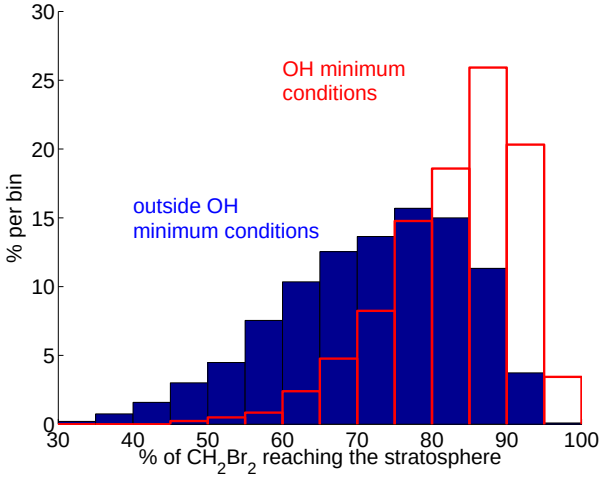

Fig. 9. Distribution of the fraction of boundary layer CH_2Br_2 surviving the transport through the troposphere for "outside minimum" conditions (filled blue) and "OH minimum" conditions (outlined red).

(Thomason and Peter, 2006; Weisenstein et al., 1997). For "OH minimum" conditions, the aerosol surface area density in the upper free troposphere drops by up to 25 % (due to less efficient conversion of SO_2 into sulfate), while that in the lowermost stratosphere increases by more than 5 % (due to increased SO_2 transport into the stratosphere and conversion into sulfate at higher altitudes).

These calculations were carried out for background SO_2 fluxes, corresponding to less than 50 ppt of SO_2 in the tropical boundary layer. The impact in the stratosphere well above the tropopause is limited because of the large and mainly unchanged contribution of COS. But anthropogenic SO_2 emissions from South East Asia and from dense ship traffic in the Pacific can substantially enhance surface SO_2 levels above background conditions, such that their relative contribution to the stratospheric sulfur budget is larger. Our findings suggest that increasing SO_2 emissions from South East Asia (Thomason and Peter, 2006) contribute to aerosol formation in the upper tropical troposphere and lower stratosphere and may contribute to the long term increase in aerosol loading observed there (Vernier et al., 2011). However, global model studies with an interactive stratospheric aerosol scheme and with a model that includes the OH minimum in the tropical West Pacific are required to quantify the effect.

Compared to background conditions, the effect of low OH values on stratospheric aerosol will be much more pronounced in the event of weak to moderate volcanic eruptions depositing much larger amounts of SO_2 into the upper troposphere from where it can be transported into the stratosphere (Hofmann et al., 2009). The presence of the OH minimum facilitates the transport of SO_2 into the stratosphere if volcanic injection occurs into the troposphere of that region. Hence, such smaller eruptions, which often do not directly inject sulfur into the stratosphere, may be more relevant for climate.

6 Discussion and conclusions

Our findings show that emissions of various chemical species in the region of the tropical West Pacific are more likely to reach the stratosphere than elsewhere. This is due to both increased lifetimes of chemical species in that geographical region and to preferred transport of air from that area into the stratosphere.

Measurements of ozone sondes, satellite instruments, lidar and FTIR instruments show a pronounced tropospheric ozone minimum in the tropical West Pacific (see Figures 4a, 5). In particular, ozone sonde measurements conducted by us during the TransBrom cruise with the RV Sonne along 140–150°E in the center of the West Pacific warm pool in October 2009 show ozone profiles below the detection limit throughout the troposphere (Fig. 1). This implies a corresponding OH minimum via Reaction R1 and R2.

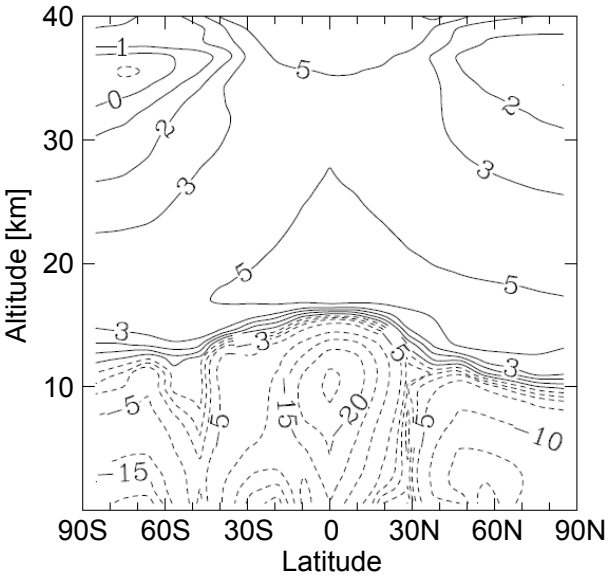

Fig. 10. Percent difference in aerosol surface area densities between runs of the 2-D AER model for "OH minimum" and "outside minimum" conditions, as a function of altitude and latitude.

In the light of the very limited availability of OH measurements in this region, we have performed simulations with the GEOS-Chem Chemistry and Transport Model for October 2009. These simulations show a pronounced minimum in the tropospheric column of OH. There is some uncertainty in this modeling result (e.g. due to uncertainties in cloud cover or water vapor), but the few existing OH measurements agree well with our model results. One particular measurement with very low OH from the STRAT campaign could be attributed to a West Pacific air mass (Fig. 2). Direct observations of OH are not available in the tropical West Pacific, but will eventually be needed to firmly establish the abundance of this key species in that region. Low OH values increase the lifetime of species that are primarily removed by reaction with OH in the troposphere.

We find that the tropical West Pacific is the major source region for stratospheric air. We performed trajectory calculations with the Lagrangian ATLAS Chemistry and Transport Model for 2002–2011 showing that air reaching the stratosphere passes through the troposphere in the same region where the inferred OH minimum is located (Figure 4d and Figure 7).

We performed conceptual model simulations that show the effect of the OH minimum on short-lived species at the example of CH_2Br_2 and SO_2. The lifetime of CH_2Br_2 increases from 55 to 188 days between OH maximum and minimum conditions, and the gas-phase lifetime of SO_2 increases from 5 to 18 days. Changes in these species are relevant, since CH_2Br_2 is one of the short-lived brominated species that contribute to the stratospheric halogen budget and is respon-

sible for part of the stratospheric ozone depletion, and SO_2 is one of the source gases of the stratospheric aerosol layer.

The tropospheric OH minimum also impacts global lifetimes of those greenhouse gases predominantly lost by chemical breakdown in the troposphere. This is the case for most of the HCFCs. The local lifetime of these species (e.g. CH_3CCl_3) is inversely proportional to OH concentrations and hence a factor of 3.5 longer in the OH minimum area as compared to outside the minimum OH region. This can increase the global lifetimes and hence the global warming potential of these species.

Direct observations of OH in the tropical West Pacific are required to more robustly assess the extent and depth of the OH minimum. At present it is unclear whether there is a relationship between global warming and possible changes in the low OH and ozone region. Changes in tropical convection due to rising sea surface temperatures, increased upwelling through the tropical tropopause, as has been suggested by some climate models (WMO, 2011), and increased anthropogenic emissions of hydrocarbons can in principle all affect the processes discussed here. Potential climate feedbacks arising from such changes need to be carefully assessed.

Appendix A

Ozonesonde measurements

Ozone soundings were carried out following standard operation procedures with sondes manufactured by EnSci Corporation attached to Graw DFM-97 radiosondes. The ozonesondes were stored and prepared in an air-conditioned room at approximately 26 °C room temperature and 60 % relative humidity. During preparation at the ground no difference in the cell current could be detected between measurements of ambient air and measurements with an ozone filter attached to the sonde. Two different ozone destruction filters were attached to the ozonesonde for all six soundings between 15° N and 8° S. These ground measurements were repeated both outside and in the air-conditioned room. The ozone destruction filters were always stored in the low relative humidity environment and one of them was never taken outside, making any adverse effect of high humidity on the efficiency of the filters very unlikely. In the stratosphere all ozonesondes measured normal tropical ozone profiles. The signal from most ozonesondes could be received by the ground station during descent after the burst of the balloon and ozone readings returned to values below the detection limit of the sensor when the sensor reached the troposphere again.

During the standard preparation of an ozonesonde at the ground electrochemical (ECC) ozone sensors exhibit a significant background current. The time evolution of that background current during the balloon ascent is not known and recommendations how to correct for the background current range from assuming a constant background throughout the sounding (recommended in the operation manual from EnSci corporation) over assuming a falloff of the background current as a function of pressure (recommended in the operation manual from Vaisala) to assuming that the background current drops to zero soon after launch (Vömel and Diaz, 2010). Figure A1 shows one example of an ozone profile from the inner tropics derived from the cell current based on all three assumptions. The real evolution of the background current is unknown at present, because it has never been measured during flight. Until such measurements are available for a wide range of meteorological conditions the unknown evolution of the background current contributes to the uncertainty of ECC ozonesonde measurements at very low ozone concentrations and actually defines the detection limit of such sensors. Once the cell current falls below the background current (that has been measured before launch) the measurement is compatible with zero ozone concentrations. For portions of the profile where the cell current is below the background current that has been measured on the ground, a robust upper limit of ozone is defined by the ozone values that are calculated directly from the cell current without subtracting any background current. Based on these considerations and typical background currents, the detection limit of ECC ozonesonde sensors is around 15 ppbv in the upper free troposphere and at the tropopause. The figures in the paper show the results based on Vaisala's recommendation for a pressure dependent background current and the shading in Fig. 1 illustrates the detection limit for typical background currents. Figure A1 shows that for most of the troposphere the ozone mixing ratios based on this method are very close to the upper limit that follows from completely ignoring the background current (the right edge of the shading).

The analysis of ozonesonde data from CEPEX was based on the subtraction of a constant background current, an approach which is now believed to result in a significant underestimation of ozone at low concentrations (Vömel and Diaz, 2010). For our measurements this approach would result in negative ozone readings throughout large parts of the middle to upper troposphere (the left edge of the shading in Fig. A1), illustrating how significantly lower the tropical measurements during TransBrom were, compared to the CEPEX measurements further east.

Acknowledgements. We thank two anonymous reviewers and in particular M. Manning for very useful comments on the original manuscript, which significantly improved the paper. We thank Ru-Shan Gao (NOAA) for his contributions and sharing his data. This work was supported by the European Community within the SHIVA project (grant no. 226224) and the StratoClim project (grant no. 603557). TransBrom was financed by the BMBF (grant no. 03G0731A). Susan Tegtmeier and Viktoria Mohr were funded by the WGL project TransBrom. We thank ECMWF for providing ERA Interim data.

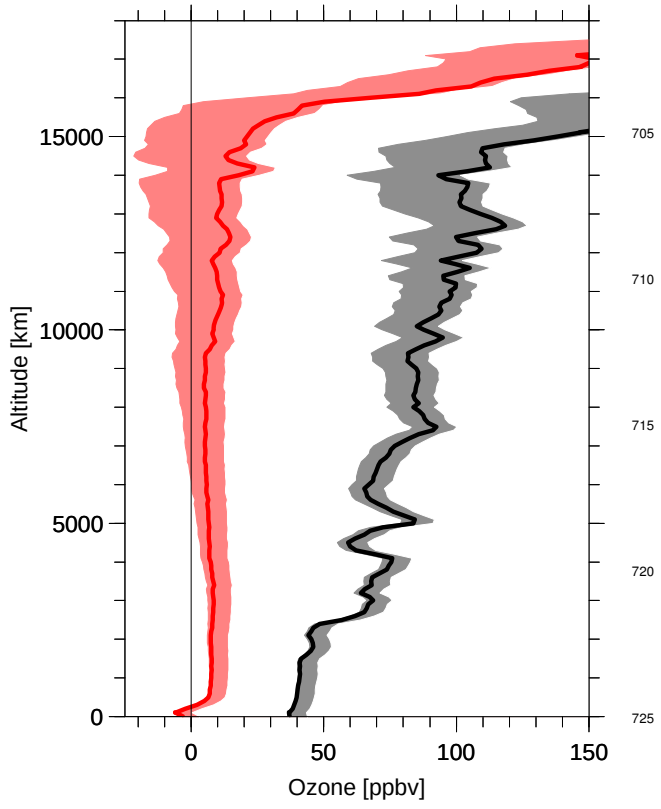

Fig. A1. Tropospheric ozone profiles at 33.5° N (black, 11 October) and at 10.5° N (red, 16 October). The shading illustrates the effect of different assumptions on the evolution of the background current during the sounding on the ozone mixing ratios calculated from the cell current. The lowest values (left hand edge of the shading) result from subtracting a constant background current, the highest values (right hand edge) from assuming that the background current drops to zero immediately after the launch, i.e. from not subtracting any background. The lines reflect the results from subtracting a pressure dependent background current (see text).

References

Aschmann, J. and Sinnhuber, B.-M.: Contribution of very short-lived substances to stratospheric bromine loading: uncertainties and constraints, Atmos. Chem. Phys., 13, 1203–1219, 2013.

Berglen, T. F., Berntsen, T. K., Isaksen, I. S. A., and Sundet, J. K.: A global model of the coupled sulfur/oxidant chemistry in the troposphere: The sulfur cycle, J. Geophys. Res., 109, D19310, doi:10.1029/2003JD003948, 2004.

Bonazzola, M. and Haynes, P. H.: A trajectory-based study of the tropical tropopause region, J. Geophys. Res., 109, D20112, doi:10.1029/2003JD004356, 2004.

Browell, E. V., Fenn, M. A., Butler, C. F., Grant, W. B., Ismail, S., Ferrare, R. A., Kooi, S. A., Brackett, V. G., Clayton, M. B., Avery, M. A., Barrick, J. D. W., Fuelberg, H. E., Maloney, J. C., Newell, R. E., Zhu, Y., Mahoney, M. J., Anderson, B. E., Blake, D. R., Brune, W. H., Heikes, B. G., Sachse, G. W., Singh, H. B., and Talbot, R. W.: Large-scale air mass characteristics observed over the remote tropical Pacific Ocean during March–April 1999: Results from PEM-Tropics B field experiment, J. Geophys. Res., 106, 32 481–32 501, 2001.

Dee, D. P., Uppala, S. M., Simmons, A. J., Berrisford, P., Poli, P., Kobayashi, S., Andrae, U., Balmaseda, M. A., Balsamo, G., Bauer, P., Bechtold, P., Beljaars, A. C. M., van de Berg, L., Bidlot, J., Bormann, N., Delsol, C., Dragani, R., Fuentes, M., Geer, A. J., Haimberger, L., Healy, S. B., Hersbach, H., Hólm, E. V., Isaksen, L., Kållberg, P., Köhler, M., Matricardi, M., McNally, A. P., Monge-Sanz, B. M., Morcrette, J.-J., Park, B.-K., Peubey, C., de Rosnay, P., Tavolato, C., Thépaut, J.-N., and Vitart, F.: The ERA-Interim reanalysis: configuration and performance of the data assimilation system, Q. J. R. Met. Soc., 137, 553–597, 2011.

Fueglistaler, S., Wernli, H., and Peter, T.: Tropical troposphere-to-stratosphere transport inferred from trajectory calculations, J. Geophys. Res., 109, D03108, doi:10.1029/2003JD004069, 2004.

Fujiwara, M., Tomikawa, Y., Kita, K., Kondo, Y., Komala, N., Saraspriya, S., Manik, T., Suripto, A., Kawakami, S., Ogawa, T., Kelana, E., Suhardi, B., Harijono, S. W. B., Kudsy, M., Sribimawati, T., and Yamanaka, M.: Ozonesonde observations in the Indonesian maritime continent: a case study on ozone rich layer in the equatorial upper troposphere, Atmos. Environ., 37, 353–362, 2003.

Gao, R. S., Fahey, D. W., Salawitch, R. J., Lloyd, S. A., Anderson, D. E., DeMajistre, R., McElroy, C. T., Woodbridge, E. L., Wamsley, R. C., Donnelly, S. G., Del Negro, L. A., Proffitt, M. H., Stimpfle, R. M., Kohn, D. W., Kawa, S. R., Lait, L. R., Loewenstein, M., Podolske, J. R., Keim, E. R., Dye, J. E., Wilson, J. C., and Chan, K. R.: Partitioning of the reactive nitrogen reservoir in the lower stratosphere of the southern hemisphere: Observations and modeling, J. Geophys. Res., 102, 3935–3949, doi:10.1029/96JD01967, 1997.

Hanisco, T. F., Lanzendorf, E. J., Wennberg, P. O., Perkins, K. K., Stimpfle, R. M., Voss, P. B., Anderson, J. G., Cohen, R. C., Fahey, D. W., Gao, R. S., Hintsa, E. J., Salawitch, R. J., Margitan, J. J., McElroy, C. T., and Midwinter, C.: Sources, Sinks, and the Distribution of OH in the Lower Stratosphere, J. Phys. Chem. A, 105, 1543–1553, 2001.

Hofmann, D., Barnes, J., O'Neill, M., Trudeau, M., and Neely, R.: Increase in background stratospheric aerosol observed with lidar at Mauna Loa Observatory and Boulder, Colorado, Geophys. Res. Lett., 36, L15808, doi:10.1029/2009GL039008, 2009.

Hossaini, R., Chipperfield, M. P., Dhomse, S., Ordóñez, C., Saiz-Lopez, A., Abraham, N. L., Archibald, A., Braesicke, P., Telford, P., Warwick, N., Yang, X., and Pyle, J.: Modelling future changes to the stratospheric source gas injection of biogenic bromocarbons, Geophys. Res. Lett., 39, L20813, doi:10.1029/2012GL053401, 2012.

Hossaini, R., Mantle, H., Chipperfield, M. P., Montzka, S. A., Hamer, P., Ziska, F., Quack, B., Krüger, K., Tegtmeier, S., Atlas, E., Sala, S., Engel, A., Bönisch, H., Keber, T., Oram, D., Mills, G., Ordóñez, C., Saiz-Lopez, A., Warwick, N., Liang, Q., Feng, W., Moore, F., Miller, B. R., Marécal, V., Richards, N. A. D., Dorf, M., and Pfeilsticker, K.: Evaluating global emission inventories of biogenic bromocarbons, Atmos. Chem. Phys., 13, 11 819–11 838, 2013.

Jaeglé, L., Jacob, D. J., Brune, W. H., and Wennberg, P. O.: Chemistry of HO_x radicals in the upper troposphere, Atmos. Environ., 35, 469–489, 2001.

Joiner, J., Schoeberl, M. R., Vasilkov, A. P., Oreopoulos, L., Platnick, S., Livesey, N. J., and Levelt, P. F.: Accurate satellite-derived estimates of the tropospheric ozone impact on the global radiation budget, Atmos. Chem. Phys., 9, 4447–4465, doi:10.5194/acp-9-4447-2009, 2009.

Kawa, S. R., Stolarski, R. S., Newman, P. A., Douglass, A. R., Rex, M., Hofmann, D. J., Santee, M. L., and Frieler, K.: Sensitivity of polar stratospheric ozone loss to uncertainties in chemical reaction kinetics, Atmos. Chem. Phys., 9, 8651–8660, 2009.

Kley, D., Crutzen, P. J., Smit, H. G. J., Vömel, H., Oltmans, S. J., Grassl, H., and Ramanathan, V.: Observations of near-zero ozone concentrations over the convective Pacific: Effects on air chemistry, Science, 274, 230–233, 1996.

Krüger, K. and Quack, B.: Introduction to special issue: the TransBrom Sonne expedition in the tropical West Pacific, Atmos. Chem. Phys., 13, 9439–9446, doi:10.5194/acp-13-9439-2013, 2013.

Krüger, K., Tegtmeier, S., and Rex, M.: Long-term climatology of air mass transport through the Tropical Tropopause Layer (TTL) during NH winter, Atmos. Chem. Phys., 8, 813–823, doi:10.5194/acp-8-813-2008, 2008.

Lawrence, M. G., Crutzen, P. J., and Rasch, P. J.: Analysis of the CEPEX ozone data using a 3D chemistry-meteorology model, Q. J. Meteorol. Soc., 125, 2987–3009, 1999.

Lelieveld, J., Dentener, F. J., Peters, W., and Krol, M. C.: On the role of hydroxyl radicals in the self-cleansing capacity of the troposphere, Atmos. Chem. Phys., 4, 2337–2344, 2004.

Levy II, H.: Normal Atmosphere: Large Radical and Formaldehyde Concentrations Predicted, Science, 173, 141–143, 1971.

Liang, Q., Stolarski, R. S., Kawa, S. R., Nielsen, J. E., Douglass, A. R., Rodriguez, J. M., Blake, D. R., Atlas, E. L., and Ott, L. E.: Finding the missing stratospheric Br_y: a global modeling study of $CHBr_3$ and CH_2Br_2, Atmos. Chem. Phys., 10, 2269–2286, 2010.

Liu, S. C., McFarland, M., Kley, D., Zafiriou, O., and Huebert, B.: Tropospheric NO_x and O_3 Budgets in the Equatorial Pacific, J. Geophys. Res., 88, 1360–1368, 1983.

Madronich, S. and Flocke, S.: The role of solar radiation in atmospheric chemistry, in: Handbook of Environmental Chemistry, edited by Boule, P., pp. 1–26, Springer-Verlag, Heidelberg, 1999.

Manning, M. R., Lowe, D. C., Moss, R. C., Bodeker, G. E., and Allan, W.: Short-term variations in the oxidizing power of the atmosphere, Nature, 436, 1001–1004, 2005.

Martinez-Aviles, M., Kreher, K., Johnston, P., Thomas, A., Hay, T., Schofield, R., and Kenntner, M.: Sources of Halogen Oxides Along the Coastline of New Zealand: A Field Measurement Study, Geophys. Res. Abstracts, 12, 673, 2010.

Montzka, S. A., Krol, M., Dlugokencky, E., Hall, B., Jöckel, P., and Lelieveld, J.: Small Interannual Variability of Global Atmospheric Hydroxyl, Science, 331, 67–69, 2011.

Naik, V., Voulgarakis, A., Fiore, A. M., Horowitz, L. W., Lamarque, J.-F., Lin, M., Prather, M. J., Young, P. J., Bergmann, D., Cameron-Smith, P. J., Cionni, I., Collins, W. J., Dalsøren, S. B., Doherty, R., Eyring, V., Faluvegi, G., Folberth, G. A., Josse, B., Lee, Y. H., MacKenzie, I. A., Nagashima, T., van Noije, T. P. C., Plummer, D. A., Righi, M., Rumbold, S. T., Skeie, R., Shindell, D. T., Stevenson, D. S., Strode, S., Sudo, K., Szopa, S., and Zeng, G.: Preindustrial to present-day changes in tropospheric hydroxyl radical and methane lifetime from the Atmospheric Chemistry and Climate Model Intercomparison Project (ACCMIP), Atmos. Chem. Phys., 13, 5277–5298, doi:10.5194/acp-13-5277-2013, 2013.

Newell, R. E. and Gould-Stewart, S.: A Stratospheric Fountain?, J. Atmos. Sci., 38, 2789–2796, 1981.

Osterman, G.: Earth Observing System (EOS) Tropospheric Emission Spectrometer (TES) Level 2 (L2) Data User's Guide, JPL Publication D-38042, http://tes.jpl.nasa.gov/documents/, 2013.

Proffitt, M. H. and McLaughlin, R. J.: Fast-response dual-beam UV-absorption ozone photometer suitable for use on stratospheric balloons, Rev. Sci. Instrum., 54, 1719–1728, 1983.

Quack, B. and Wallace, D. W. R.: Air-sea flux of bromoform: Controls, rates, and implications, Global Biogeochem. Cycles, 17, 1023, doi:10.1029/2002GB001890, 2003.

Ridder, T., Gerbig, C., Notholt, J., Rex, M., Schrems, O., Warneke, T., and Zhang, L.: Ship-borne FTIR measurements of CO and O_3 in the Western Pacific from 43° N to 35° S: an evaluation of the sources, Atmos. Chem. Phys., 12, 815–828, doi:10.5194/acp-12-815-2012, 2012.

Rohrer, F. and Berresheim, H.: Strong correlation between levels of tropospheric hydroxyl radicals and solar ultraviolet radiation, Nature, 442, 184–187, 2006.

Sander, S. P., Abbatt, J., Barker, J. R., Burkholder, J. B., Friedl, R. R., Golden, D. M., Huie, R. E., Kolb, C. E., Kurylo, M. J., Moortgat, G. K., Orkin, V. L., and Wine, P. H.: Chemical kinetics and photochemical data for use in atmospheric studies, Evaluation Number 17, JPL Publication 10-06, Jet Propulsion Laboratory, California Institute of Technology, Pasadena, 2011.

Scott, S. G., Bui, T. P., Chan, K. R., and Bowen, S. W.: The meteorological measurement system on the NASA ER-2 aircraft, J. Atmos Oceanic Technol., 7, 525–540, 1990.

Solomon, S., Thompson, D. W. J., Portmann, R. W., Oltmans, S. J., and Thompson, A. M.: On the distribution and variability of ozone in the tropical upper troposphere: Implications for tropical deep convection and chemical-dynamical coupling, Geophys. Res. Lett., 32, L23813, doi:10.1029/2005GL024323, 2005.

Solomon, S., Daniel, J. S., Neely III, R. R., Vernier, J.-P., Dutton, E. G., and Thomason, L. W.: The Persistently Variable "Background" Stratospheric Aerosol Layer and Global Climate Change, Science, 333, 866–870, 2011.

Stevenson, D. S., Dentener, F. J., Schultz, M. G., Ellingsen, K., van Noije, T. P. C., Wild, O., Zeng, G., Amann, M., Atherton, C. S., Bell, N., Bergmann, D. J., Bey, I., Butler, T., Cofala, J., Collins, W. J., Derwent, R. G., Doherty, R. M., Drevet, J., Eskes, H. J., Fiore, A. M., Gauss, M., Hauglustaine, D. A., Horowitz, L. W., Isaksen, I. S. A., Krol, M. C., Lamarque, J.-F., Lawrence, M. G., Montanaro, V., Müller, J.-F., Pitari, G., Prather, M. J., Pyle, J. A., Rast, S., Rodriguez, J. M., Sanderson, M. G., Savage, N. H., Shindell, D. T., Strahan, S. E., Sudo, K., and Szopa, S.: Multimodel ensemble simulations of present-day and near-future tropospheric ozone, J. Geophys. Res., 111, D08301, doi:10.1029/2005JD006338, 2006.

Takashima, H., Shiotani, M., Fujiwara, M., Nishi, N., and Hasebe, F.: Ozonesonde observations at Christmas Island (2°N, 157°W) in the equatorial central Pacific, J. Geophys. Res., 113, D10112, doi:10.1029/2007JD009374, 2008.

Tan, D., Faloona, I., Simpas, J. B., Brune, W., Olson, J., Crawford, J., Avery, M., Sachse, G., Vay, S., Sandholm, S., Guan, H.-W., Vaughn, T., Mastromarino, J., Heikes, B., Snow, J., Podolske, J.,

and Singh, H.: OH and HO_2 in the tropical Pacific: Results from PEM-Tropics B, J. Geophys. Res., 106, 32 667–32 681, 2001.

Thomason, L. and Peter, T.: Assessment of Stratospheric Aerosol Properties, SPARC Report No. 4, WMO/TD-No. 1295, http://www.sparc-climate.org, 2006.

Vernier, J. P., Thomason, L. W., Pommereau, J.-P., Bourassa, A., Pelon, J., Garnier, A., Hauchecorne, A., Blanot, L., Trepte, C., Degenstein, D., and Vargas, F.: Major influence of tropical volcanic eruptions on the stratospheric aerosol layer during the last decade, Geophys. Res. Lett., 38, L12807, doi:10.1029/2011GL047563, 2011.

Vömel, H. and Diaz, K.: Ozone sonde cell current measurements and implications for observations of near-zero ozone concentrations in the tropical upper troposphere, Atmos. Meas. Tech., 3, 495, doi:10.5194/amt-3-495-2010, 2010.

Warwick, N. J., Pyle, J. A., Carver, G. D., Yang, X., Savage, N. H., O'Connor, F. M., and Cox, R. A.: Global modeling of biogenic bromocarbons, J. Geophys. Res., 111, D24305, doi:10.1029/2006JD007264, 2006.

Weisenstein, D. K., Yue, G. K., Ko, M. K. W., Sze, N.-D., Rodriguez, J. M., and Scott, C. J.: A two-dimensional model of sulfur species and aerosols, J. Geophys. Res., 102, 13 019–13 035, 1997.

Wennberg, P. O., Cohen, R. C., Hazen, N. L., Lapson, L. B., Allen, N. T., Hanisco, T. F., Oliver, J. F., Lanham, N. W., Demusz, J. N., and Anderson, J. G.: Aircraft-borne, laser-induced fluorescence instrument for the in situ detection of hydroxyl and hydroperoxyl radicals, Rev. Sci. Instrum., 65, 1858–1876, 1994.

WMO: World Meteorological Organization (WMO) / United Nations Environment Programme (UNEP), Scientific assessment of ozone depletion: 2010, Global Ozone Research and Monitoring Project – Report No. 52, 2011.

Wohltmann, I. and Rex, M.: The Lagrangian chemistry and transport model ATLAS: validation of advective transport and mixing, Geosci. Model Dev., 2, 153–173, doi:10.5194/gmd-2-153-2009, 2009.

Wohltmann, I., Lehmann, R., and Rex, M.: The Lagrangian chemistry and transport model ATLAS: simulation and validation of stratospheric chemistry and ozone loss in the winter 1999/2000, Geosci. Model Dev., 3, 585–601, doi:10.5194/gmd-3-585-2010, 2010.

Ziemke, J. R., Chandra, S., Duncan, B. N., Froidevaux, L., Bhartia, P. K., Levelt, P. F., and Waters, J. W.: Tropospheric ozone determined from Aura OMI and MLS: Evaluation of measurements and comparison with the Global Modeling Initiative's Chemical Transport Model, J. Geophys. Res., 111, D19303, doi:10.1029/2006JD007089, 2006.